Monthly Notices of the ROYAL ASTRONOMICAL SOCIETY
MNRAS **450,** 1900–1915 (2015) doi:10.1093/mnras/stv716

Chemical abundances and kinematics of 257 G-, K-type field giants. Setting a base for further analysis of giant-planet properties orbiting evolved stars⋆

V. Zh. Adibekyan,[1]† L. Benamati,[1,2] N. C. Santos,[1,2] S. Alves,[3,4] C. Lovis,[5] S. Udry,[5] G. Israelian,[6,7] S. G. Sousa,[1] M. Tsantaki,[1,2] A. Mortier,[8] A. Sozzetti[9] and J. R. De Medeiros[10]

[1]*Instituto de Astrofísica e Ciência do Espaço, Universidade do Porto, CAUP, Rua das Estrelas, PT4150-762 Porto, Portugal*
[2]*Departamento de Física e Astronomia, Faculdade de Ciências da Universidade do Porto, PT4150-762 Porto, Portugal*
[3]*Instituto de Astrofísica, Pontificia Universidad Católica de Chile, Av. Vicuña Mackenna 4860, 782-0436 Macul, Santiago, Chile*
[4]*CAPES Foundation, Ministry of Education of Brazil, 70040-020 Brasília/DF, Brazil*
[5]*Observatoire de Genève, Universit de Genve, 51 ch. des Maillettes, CH-1290 Sauverny, Switzerland*
[6]*Instituto de Astrofísica de Canarias, E-38200 La Laguna, Tenerife, Spain*
[7]*Departamento de Astrofísica, Universidad de La Laguna, E-38206 La Laguna, Tenerife, Spain*
[8]*SUPA, School of Physics and Astronomy, University of St Andrews, St Andrews KY16 9SS, UK*
[9]*INAF – Osservatorio Astrofisico di Torino, I-10025 Pino Torinese, Italy*
[10]*Departamento de Física Teórica e Experimental, Universidade Federal do Rio Grande do Norte, Campus Universitário Lagoa Nova, 59072-970 Natal, RN, Brazil*

Accepted 2015 March 27. Received 2015 March 25; in original form 2015 January 26

ABSTRACT

We performed a uniform and detailed abundance analysis of 12 refractory elements (Na, Mg, Al, Si, Ca, Ti, Cr, Ni, Co, Sc, Mn, and V) for a sample of 257 G- and K-type evolved stars from the CORALIE planet search programme. To date, only one of these stars is known to harbour a planetary companion. We aimed to characterize this large sample of evolved stars in terms of chemical abundances and kinematics, thus setting a solid base for further analysis of planetary properties around giant stars. This sample, being homogeneously analysed, can be used as a comparison sample for other planet-related studies, as well as for different type of studies related to stellar and Galaxy astrophysics. The abundances of the chemical elements were determined using an local thermodynamic equilibrium (LTE) abundance analysis relative to the Sun, with the spectral synthesis code MOOG and a grid of Kurucz ATLAS9 atmospheres. To separate the Galactic stellar populations, both a purely kinematical approach and a chemical method were applied. We confirm the overabundance of Na in giant stars compared to the field FGK dwarfs. This enhancement might have a stellar evolutionary character, but departures from LTE may also produce a similar enhancement. Our chemical separation of stellar populations also suggests a 'gap' in metallicity between the thick-disc and high-α metal-rich stars, as previously observed in dwarfs sample from HARPS. The present sample, as most of the giant star samples, also suffers from the $B - V$ colour cut-off, which excludes low-log g stars with high metallicities, and high-log g star with low [Fe/H]. For future studies of planet occurrence dependence on stellar metallicity around these evolved stars, we suggest to use a subsample of stars in a 'cut-rectangle' in the log g–[Fe/H] diagram to overcome the aforementioned issue.

Key words: methods: observational – techniques: spectroscopic – stars: abundances – planetary systems.

1 INTRODUCTION

The precise chemical and kinematic characterization of intermediate-mass, evolved stars is very important for different fields of both Galactic and stellar astronomy, and the emerging field of planetary sciences.

⋆Based on observations collected at the Paranal Observatory, ESO (Chile) with the Ultra-violet and Visible Echelle Spectrograph (UVES) of the VLT, under programmes 085.C-0062 and 086.C-0098.

†E-mail: vadibekyan@astro.up.pt

Many studies observed significant differences in chemical abundances between main-sequence dwarf and evolved stars (e.g. Friel et al. 2003; Jacobson, Friel & Pilachowski 2007; Villanova, Carraro & Saviane 2009; Santrich, Pereira & Drake 2013). While these differences for some elements might by astrophysical, having a stellar evolutionary character (e.g. Tautvaišiene et al. 2005, for sodium), several authors however suggested that the differences may arise also in the analysis, being dependent on the particular method and line-list used (e.g. Santos et al. 2009). Along the same line, one should consider also non-local thermodynamic equilibrium (non-LTE) effects which are stronger for giants than for dwarfs and may have a strong influence on the analysis (e.g. Bergemann et al. 2013; Alexeeva, Pakhomov & Mashonkina 2014; Bergemann, Kudritzki & Davies 2014).

Understanding the mentioned issues, will not only allow us to improve of stellar atmosphere models, but also will have very important implications in several fields of astrophysics. For instance, it would help us shed light on the statistical and evolutionary properties of planetary systems around giant stars, e.g. on the possible absence of the correlation between stellar metallicity and formation efficiency of giant planets (e.g. Pasquini et al. 2007; Takeda, Sato & Murata 2008; Ghezzi et al. 2010; Maldonado, Villaver & Eiroa 2013; Mortier et al. 2013c; Jofré et al. 2015)[1] which was found for main-sequence dwarf stars (e.g. Gonzalez 1997; Santos, Israelian & Mayor 2001, 2004; Fischer & Valenti 2005; Johnson et al. 2010; Sousa et al. 2011; Mortier et al. 2013b).

Several explanations have been suggested for the aforementioned lack of metallicity enhancement for giant stars hosting a giant planet. Higher stellar mass of giants may compensate the lack of metals (e.g. Ghezzi et al. 2010), possible spectroscopic analysis issues in giant stars (e.g. Hekker & Meléndez 2007; Santos et al. 2009), selection biases in giant star samples (Mortier et al. 2013c). However, one should note that some studies reported an enhanced metallicity of giant stars with planets, but with small samples of planet hosts (Hekker & Meléndez 2007; Quirrenbach, Reffert & Bergmann 2011). We refer the reader to Alves et al. (2015, and reference therein) for more detailed review on the topic.

In this paper, we focus on the chemical and kinematic properties of a sample of 257 field giant stars which are observed within the context of the CORALIE extrasolar planet search programme. The main characteristics of the sample along with the homogeneously derived stellar atmospheric parameters are presented in a parallel paper (Alves et al. 2015). The uniform chemical analysis of these giant stars is very important to explore the specific chemical requirements for the formation and evolution of planetary systems around them. The paper is organized as follows: in Section 2, we briefly introduce the sample used in this work. The method of the chemical abundance determination and analysis will be explained in Section 3. The distinction of different Galactic stellar populations and kinematic properties of the stars are presented in Section 4. Then, after discussing the metallicity distribution of the stars in Section 5, we summarize our main results in Section 6.

2 SAMPLE DESCRIPTION AND STELLAR PARAMETERS

Our sample comprises 257 G- and K-type evolved stars that are being surveyed for planets in the context of the CORALIE (Udry et al. 2000) extrasolar planet search programme. High-resolution and high signal-to-noise (S/N) spectra were obtained using the UVES spectrograph. Precise stellar parameters for the entire sample were determined in Alves et al. (2015) by using the same spectra as we did for this study. The spectroscopic stellar parameters and metallicities were derived by imposing excitation and ionization equilibrium. The spectroscopic analysis was completed assuming LTE with a grid of Kurucz atmosphere models (Kurucz 1993), and the 2002 version of the MOOG[2] radiative transfer code (Sneden 1973). We refer the reader to Alves et al. (2015) and Sousa (2014) for details.

Alves et al. (2015) derived the atmospheric parameters by using three different line-lists of Fe I and Fe II (Hekker & Meléndez 2007; Sousa et al. 2008; Tsantaki et al. 2013). Whilst showing that the use of different line-lists gives compatible results, the parameters derived following Tsantaki et al. (2013) were adopted, so we also do for the rest of the present paper.

The stars in the sample have effective temperatures $4700 \lesssim T_{\rm eff} \lesssim 5600$ K, surface gravities $2.2 \lesssim \log g \lesssim 3.7$ dex, microturbulence $1 \lesssim \xi_{\rm t} \lesssim 3.2$ km s^{-1}and they lie in the metallicity range of $-0.75 \lesssim$ [Fe/H] $\lesssim 0.3$ dex.

3 CHEMICAL ABUNDANCES

For the abundance derivation, we closely followed the method described in Adibekyan et al. (2012a).

3.1 Selection of the lines and abundance derivation

The initial line-list and the atomic data were taken from Adibekyan et al. (2012a) and Neves et al. (2009). Neves et al. (2009) provided the astrophysical (calibrated) oscillator strength and solar equivalent widths of the lines. Since the spectra of cool evolved stars are more line crowded (which cause strong blending) compared to their unevolved hotter counterparts, we aimed to carefully select a subset of unblended lines from Adibekyan et al. (2012a). For this purpose, as a reference we used a very high S/N and high-resolution archival spectrum of the K-type giant Arcturus observed with the NARVAL spectrograph (Mortier et al. 2013c). We measured the equivalent widths (EWs) of the selected lines both manually, using a Gaussian-fitting procedure within the IRAF[3] `splot` task, and automatically, by using the ARES[4] code (Sousa et al. 2007). We calculated the mean relative difference $((\mathrm{EW_{ARES}} - \mathrm{EW_{IRAF}})/\ \mathrm{EW_{IRAF}})$ and standard deviation of the relative difference of the EW measurements and applied 2σ-clipping. We repeated this procedure a second time after the outliers were excluded. Finally, 118 lines out of 164 were left that show a relative difference in EW of less than 15 per cent. These lines were once again checked by eye within IRAF to make sure that they are not blended and hence the correspondence between the EW measurements is not by chance.[5]

After selecting the isolated lines, the abundances for 12 elements (Na, Mg, Al, Si, Ca, Ti, Cr, Ni, Co, Sc, Mn, and V) were determined

[1] Indeed, Reffert et al. (2015) claims a strong evidence for a planet–metallicity correlation for giant planet host stars.

[2] The source code of MOOG can be downloaded at http://www.as.utexas.edu/~chris/moog.html

[3] IRAF is distributed by National Optical Astronomy Observatories, operated by the Association of Universities for Research in Astronomy, Inc., under contract with the National Science Foundation, USA.

[4] The ARES code can be downloaded at http://www.astro.up.pt/~sousasag/ares

[5] The line-list is available at the CDS: http://cdsarc.u-strasbg.fr/viz-bin/qcat?J/MNRAS/

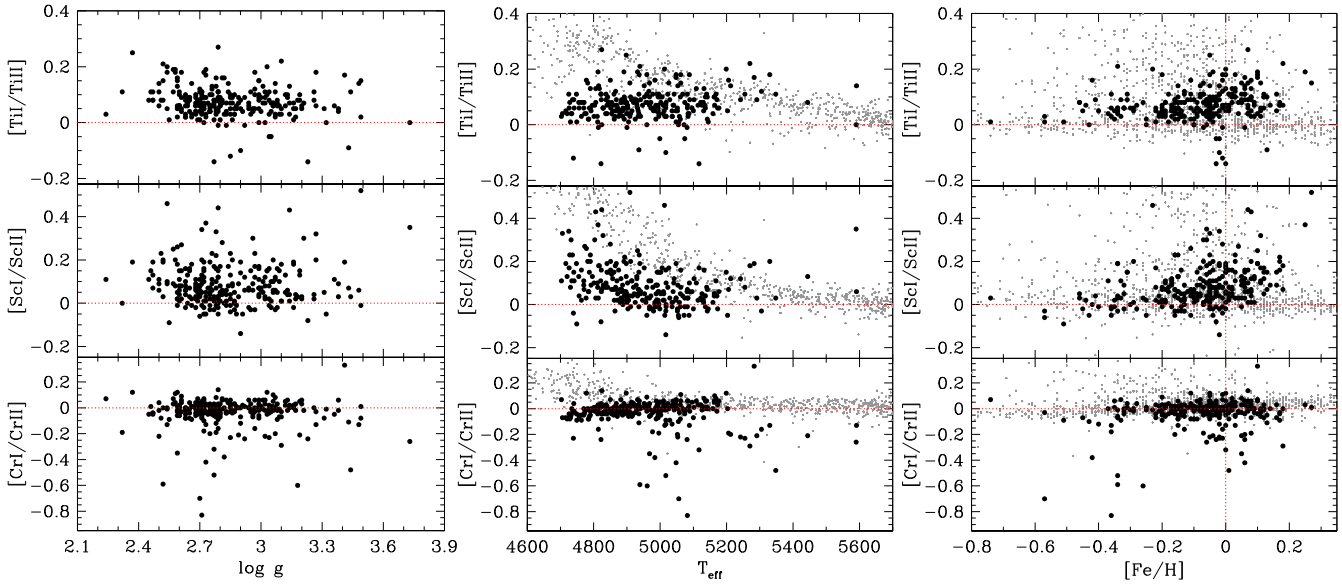

Figure 1. [Cr I/Cr II], [Sc I/Sc II], and [Ti I/Ti II] as a function of atmospheric parameters for our sample of evolved stars (black points) and for the sample of FGK dwarf stars from Adibekyan et al. (2012a, grey dots).

using an LTE analysis relative to the Sun with the 2010 version of the MOOG (Sneden 1973) and a grid of Kurucz ATLAS9 plane-parallel model atmospheres with no α-enhancement. The reference abundances used in the abundance analysis were taken from Anders & Grevesse (1989). We note that our analysis is differential and the source of the reference abundances is not crucial. For the automatic EW measurements, we used ARES for which the input parameters were the same as in Sousa et al. (2008) and the *rejt* parameter is calculated following the procedure discussed in Mortier et al. (2013c). The EWs of all the lines used in the derivation of the abundances for all studied stars is available at CDS.

The final abundance for each star and element was calculated to be the average value of the abundances given by all lines detected in a given star and element. Individual lines for a given star and element with a line dispersion more than a factor of 2 higher than the rms were excluded. In this way we avoided the errors caused by bad pixels, cosmic rays, or other unknown effects. A sample of our results for three stars is presented in Table 2 and the complete results are available at the CDS.

3.2 Uncertainties

Since the abundances were determined via the measurement of EWs and using already determined stellar parameters, the errors might come from the EW measurements, from the errors in the atomic parameters, and from the uncertainties of the atmospheric parameters that were used to make an atmosphere model. In addition to the above-mentioned errors, one should add systematic errors that can occur due to non-LTE or granulation (3D) effects. To minimize the errors, it is very important to use high-quality data and as many lines as possible for each element.

We followed Adibekyan et al. (2012a) for the calculation of the errors. In short, we first varied the model parameters by an amount of their 1σ errors available for each star and calculated the abundance differences between the values obtained with and without varying the parameter. Then we evaluated the errors in the abundances of all elements [*X*/H], adding quadratically the line-to-line scatter errors and errors induced by uncertainties in the model atmosphere parameters. In cases when only one line used to derive the abundances, a typical 0.1 dex error for line-to-line scatter was assumed. For our sample stars, the errors induced by uncertainties in the parameters of model atmosphere varies from about 0.02 dex (for Si I) to ≈0.06 dex (for V I) and in general are smaller than the line-to-line scatter errors. The final errors for the studied elements are smallest for Al I (≈0.04 dex) and largest for V I (≈0.14 dex).

3.3 Testing the validity of the stellar parameters

Although Alves et al. (2015) have shown that the stellar parameters in general agree very well with the literature data, the consistency does not always imply correctness. Moreover, the stellar parameters were derived by completing an LTE abundance analysis and by using only iron lines. To check the validity limit of the adopted methodology in terms of stellar parameter ranges, we tested our results in two ways (see also Adibekyan et al. 2012a).

First, in Fig. 1, we plot the [Cr I/Cr II], [Sc I/Sc II], and [Ti I/Ti II] as a function of the stellar parameters to ensure that the ionization equilibrium enforced on the Fe II lines (Alves et al. 2015) is acceptable to other elements. For comparison, the field FGK dwarf stars from Adibekyan et al. (2012a) are presented. Most of the trends are nearly flat around zero in contradiction to their unevolved counterparts for which a gradual increase with decreasing $T_{\rm eff}$ was observed. For our stars, only an increase of [Sc I/Sc II] ratio can be seen with the decrease of $T_{\rm eff}$. However, the results obtained for Sc I and Cr II should be considered with caution since their abundances have been derived by using only one line. From the figure, one can notice a small offset from zero for [Ti I/Ti II] ratio and [Sc I/Sc II]. These positive offsets probably do not have relation to the non-LTE effects as discussed in Bergemann (2011) for [Ti I/Ti II] and still need to be understood.

Tsantaki et al. (2013) showed that by correcting stellar parameters (mainly $T_{\rm eff}$), using carefully selected line-list especially designed for cool stars, the observed trends of [*X* I/*X* II] with stellar parameters get flatter. For example, an overestimation of $T_{\rm eff}$ for cool stars might

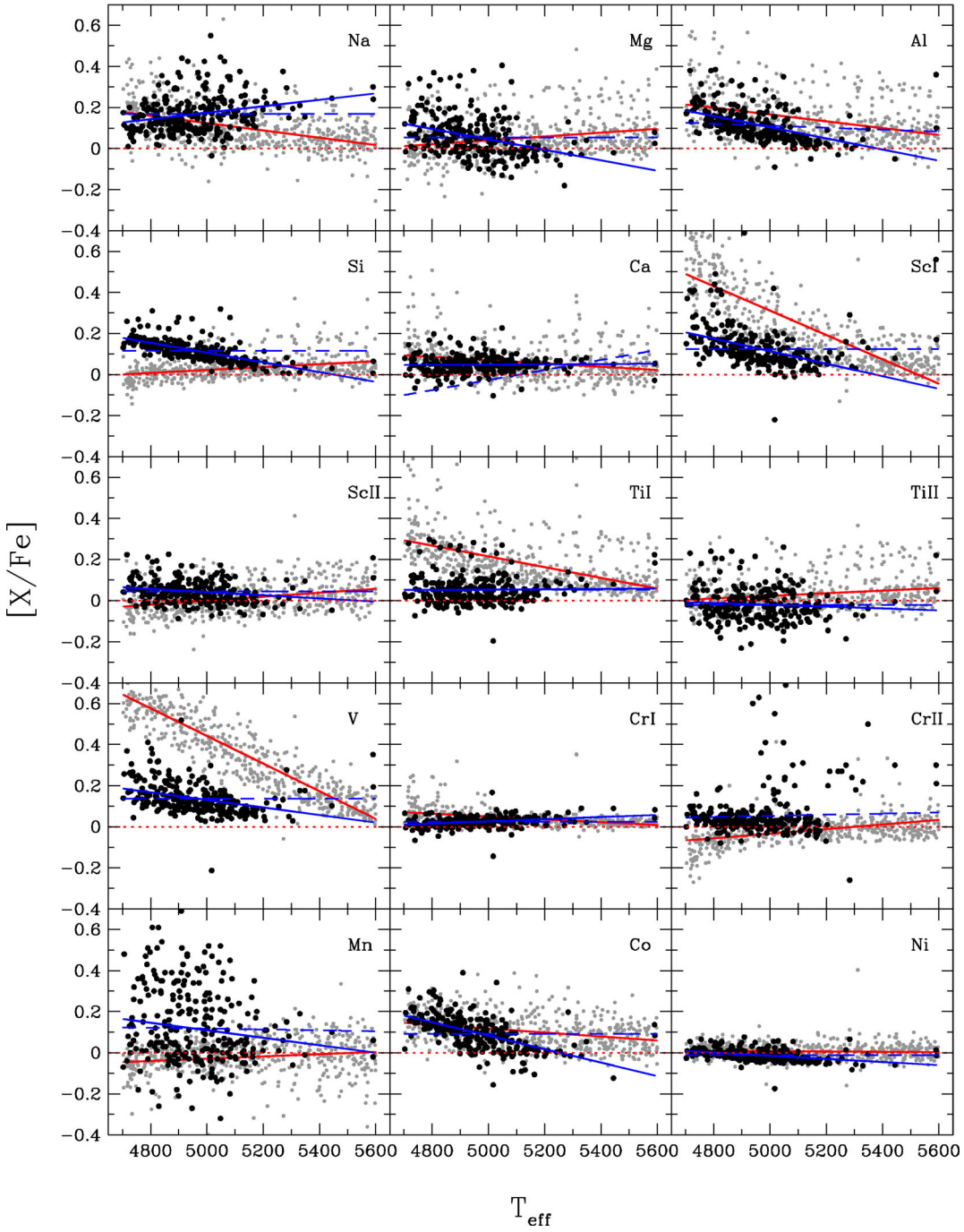

Figure 2. [*X*/Fe] versus $T_{\rm eff}$ plots. The black dots represent the stars of the sample and the grey small dots represent stars from Adibekyan et al. (2012a). The blue and red solid lines depict the linear fits of the current data and the data from Adibekyan et al. (2012a), respectively. The blue dashed line is the fit of our data after correcting for the trend with $T_{\rm eff}$. Each element is identified in the upper-right corner of the respective plot.

cause of the trends. The dependence of the abundances of ionized and neutral species on the surface gravity is also discussed in Mortier et al. (2013a).

Another way of testing the stellar parameters is to plot [*X*/Fe] against $T_{\rm eff}$ (Fig. 2). For the comparison, the dwarf sample of Adibekyan et al. (2012a) is also presented. Stellar evolutionary models do not suggest significant trends of these ratios with $T_{\rm eff}$. However, for several elements we detected significant trends. To evaluate the significance of the trends, we performed a linear fit and followed the procedure described in Figueira et al. (2013). In short, first, we obtained the zero-centred distribution of the correlation coefficient by randomly bootstrapping (building random samples by shuffling the parameters among the observed set of parameters) the observed data pairs 10^4 times. Then we calculated the correlation coefficient for each of these uncorrelated data sets and then the average and standard deviation of these values. By assuming a Gaussian distribution for R (correlation coefficient), we calculated the probability that the R of the original data set was obtained by pure chance. The significance of the trends and the slopes are presented in Table 1. From the figure, one can see that for most cases

Table 1. The slope, correlation coefficient, and the significance of the [*X*/Fe] linear trends with the $T_{\rm eff}$.

Elem	Slope	R^2	N	z-score
Na I	$1.62 \pm 0.36 \times 10^{-4}$	0.72×10^{-1}	256	4.3
Mg I	$-2.51 \pm 0.38 \times 10^{-4}$	0.14×10^{0}	257	6.1
A II	$-2.69 \pm 0.29 \times 10^{-4}$	0.24×10^{0}	257	7.9
Si I	$-2.39 \pm 0.16 \times 10^{-4}$	0.45×10^{0}	257	11.0
Ca I	$0.61 \pm 1.80 \times 10^{-5}$	0.44×10^{-3}	257	0.3
Sc I	$-3.00 \pm 0.34 \times 10^{-4}$	0.23×10^{0}	255	7.6
Sc II	$-0.78 \pm 0.23 \times 10^{-4}$	0.43×10^{-1}	257	3.2
Ti I	$0.81 \pm 2.94 \times 10^{-5}$	0.29×10^{-3}	257	0.2
Ti II	$-0.44 \pm 0.34 \times 10^{-4}$	0.64×10^{-2}	257	1.2
V I	$-1.79 \pm 0.29 \times 10^{-4}$	0.13×10^{0}	256	5.9
Cr I	$0.56 \pm 0.10 \times 10^{-4}$	0.98×10^{-1}	257	4.9
Cr II	$1.33 \pm 0.34 \times 10^{-4}$	0.57×10^{-1}	246	3.6
Mn I	$1.33 \pm 0.34 \times 10^{-4}$	0.57×10^{-1}	247	2.3
Co I	$-0.32 \pm 0.03 \times 10^{-3}$	0.33×10^{0}	257	9.2
Ni I	$-0.78 \pm 0.11 \times 10^{-4}$	0.16×10^{0}	257	6.3

the trends are less steep compared to those observed for the dwarfs,[6] which in turn speaks about the correctness of the stellar parameters used to derive the abundances.

Adibekyan et al. (2012a) already discussed several possible reasons for the observed trends of [X I/X II] with stellar parameters, and [*X*/Fe] with $T_{\rm eff}$[7] and concluded that the observed trends are probably not an effect of stellar evolution, and uncertainties in atmospheric models are the dominant effect in the measurements. The authors afterwards removed the $T_{\rm eff}$ trend as it was done also in other works (e.g. Valenti & Fischer 2005; Petigura & Marcy 2011).

Since by fitting the data and simply subtracting the fit would force the mean [*X*/Fe] to zero (which is an non-physical situation), Adibekyan et al. (2012a) added a constant term chosen so that the correction is zero at solar temperature. In our case, the stars are cooler and their temperatures do not reach the solar temperature so we decided to apply another approach. In this case, the constant term was chosen so that the correction is zero at $T_{\rm eff} = 4960$ K, which is the mean temperature of our sample stars. However, we appreciate the fact that this approach and the choice of the constant term is arbitrary. For this reason, we decide to use the original (before detrending) chemical abundances for the rest of our study.

The dependence of [*X*/Fe] on stellar gravity and microturbulence and metallicity is shown in Fig. B1, Fig. B2, and Fig. 3, respectively. For most of the species, we did not observe a trend with $\xi_{\rm t}$ and $\log g$, and some of the observed trends probably reflect the correlation of $T_{\rm eff}$ with other stellar parameters (see Fig. A1).

As a final check, we compare our derived abundances with those obtained by Liu et al. (2007). We note that this is the only literature source where we find enough stars (14 stars) in common to compare. We found very good agreement for all the species except vanadium: Δ[Na/H] $= 0.02 \pm 0.12$, Δ[Mg/H] $= -0.06 \pm 0.12$, Δ[Al/H] $= 0.05 \pm 0.04$, Δ[Ca/H] $= 0.03 \pm 0.06$, Δ[Si/H] $= 0.03 \pm 0.03$, Δ[Ti/H] $= 0.04 \pm 0.08$, Δ[Ni/H] $= -0.01 \pm 0.05$, and Δ[V/H] $= 0.19 \pm 0.05$.[8]

[6] Note that the stellar parameters for the dwarfs were not derived by using the Tsantaki et al. (2013) line-list which is especially designed for cool stars.
[7] Note that the Adibekyan et al. (2012a) sample essentially consists of dwarfs.
[8] $\Delta[X/H] = [X/H]_{\rm our} - [X/H]_{\rm theirs}$.

The [*X*/H] abundances of all the stars before and after correction (if the significance of the correlation is above 3σ) for the $T_{\rm eff}$ trends are available at the CDS (see also Table 2).

3.4 [*X*/Fe] versus [Fe/H] relation. Galactic chemical evolution

The [*X*/Fe] versus [Fe/H] relation plot is traditionally used to study the Galactic chemical evolution because iron is a good chronological indicator of nucleosynthesis. In Fig. 3, we present the dependence of [*X*/Fe] on metallicity for our sample of giant stars and for FGK dwarf stars from Adibekyan et al. (2012a).[9] In the figure, we also showed the average value of [*X*/Fe] for stars in the metallicity range of 0.0 ± 0.1 dex, where the Galactic chemical evolution effects are small. As one can see, for all the elements the general behaviour of [*X*/Fe] with the metallicity is similar for giant and dwarf stars, and reflects the Galactic chemical evolution in the solar neighbourhood. However, one can also clearly notice that, for some elements (Co, Na, V, Mn, Al, and Si) while the Galactic chemical evolution trends are similar, they are shifted: for giant stars having higher [*X*/Fe] values at a fixed metallicity. The largest offset is seen for Na and Mn, and a bit less in Si and Al. In general, Na and Al are not good tracers of chemical evolution and affected by internal mixing processes in the stars. The Mn abundance was obtained by using only one line and it should be considered with caution. Moreover, the scatter in [Mn/Fe] is very high, indicating unrealistic abundances for some fraction of the stars.

Overabundances of sodium and aluminium (also silicon in some cases) in open cluster giants (compared to the abundances of dwarfs) were already observed by several authors (e.g. Friel et al. 2003; Friel, Jacobson & Pilachowski 2005; Tautvaišiene et al. 2005; Jacobson et al. 2007; Villanova et al. 2009; Santrich et al. 2013). In most of these studies, the trends were explained as a stellar evolutionary effect, due to the deep mixing produced by the hydrogen burning cycle, after stars have left the main sequence. For a complete picture, one should perform thorough analysis taking into account the non-LTE effects which are stronger for giants stars and also the systematic errors which might arise due to particular spectroscopic analysis method used. For example, it is well known that sodium lines suffer from non-LTE effects which lead to an overestimation of the Na abundances (e.g. Alexeeva et al. 2014). In our analysis, we used two sodium lines (at 6154.23 and 6160.75 Å) which were studied for non-LTE effects in Alexeeva et al. (2014). The average EWs of these lines were ∼70 mÅ for 6154.23 Å, and ∼80 mÅ for the 6160.75Å line. According to Alexeeva et al., the non-LTE correction for our stars should be from −0.1 to −0.15 dex, which is close to the difference in [Na/Fe] between giants and dwarfs observed in this study.

The difference in Al abundances ([Al/Fe]) between giants and dwarfs obtained for solar-metallicity stars is not large (0.07 dex – about 1σ scatter), but seems to increase at lower metallicities. However, it should be noted that direct comparison of the abundance ratios at lower metallicities is not straightforward, since the Galactic chemical evolution effects and the relative fraction of thin- and thick-disc stars can be dominant. Several authors studied the non-LTE effects on the formation of Al lines (e.g. Baumueller & Gehren 1996, 1997; Menzhevitski, Shimansky & Shimanskaya 2012). They showed that the non-LTE correction of the Al abundances, derived from the subordinate doublet λλ 6696.03, 6698.68 Å, is very small

[9] Only stars with $T_{\rm eff} = {\rm T}_{\odot} \pm 500$ K are presented, because of the highest accuracy in the parameters and chemical abundances in these stars.

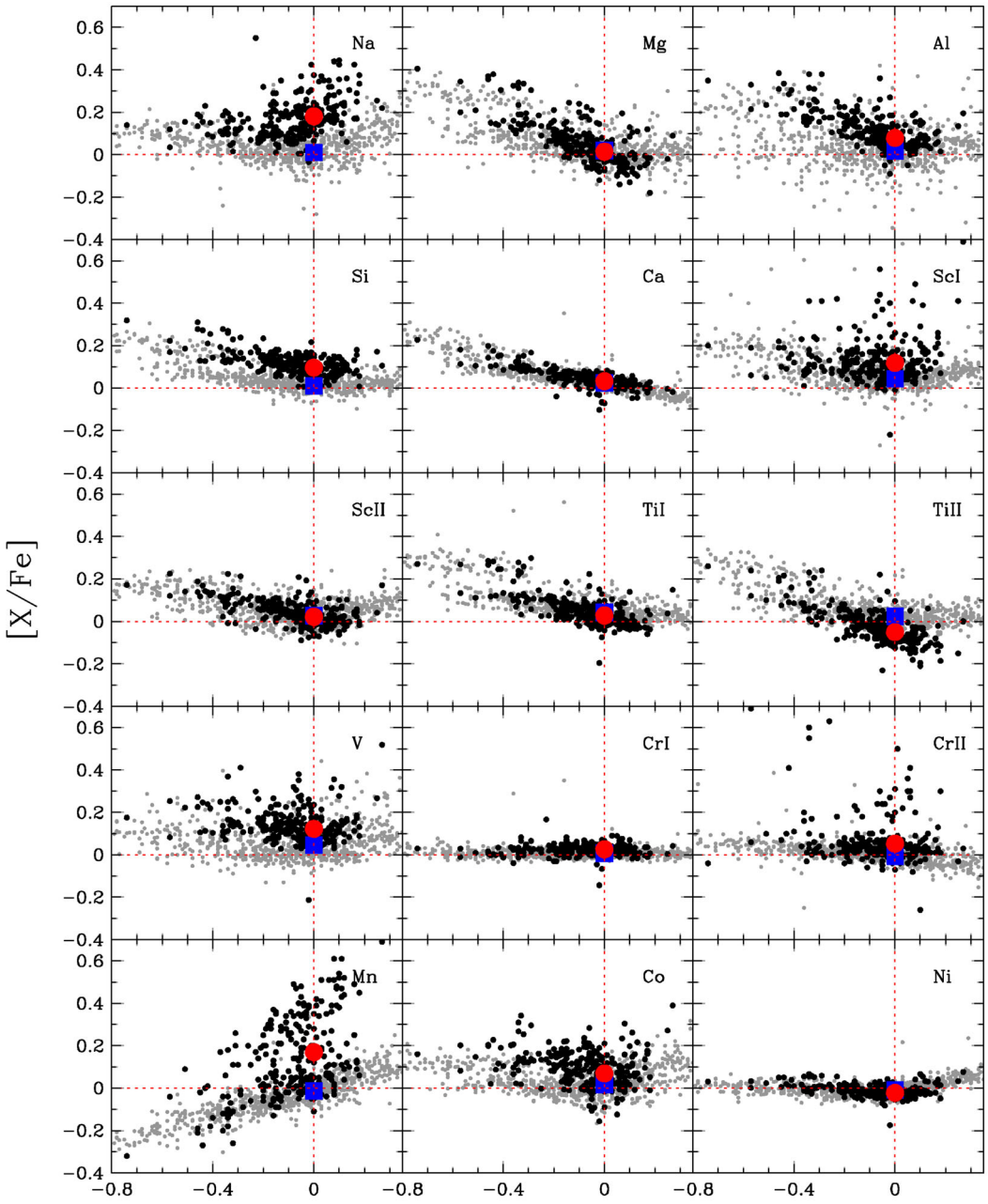

Figure 3. [*X*/Fe] versus [Fe/H] plots. The black dots represent the stars of the sample and the grey small dots represent stars from Adibekyan et al. (2012a) with $T_{\rm eff} = T_{\odot} \pm 500$ K. The red circle and blue square show the average [*X*/Fe] value of stars with [Fe/H] $= 0.0 \pm 0.1$ dex. Each element is identified in the upper-right corner of the respective plot.

Table 2. Sample table of the derived abundances of the elements, rms, total error, and number of measured lines for each star.

Star	...	[Si I/H]	rms	err	$[\text{Si I/H}]^{*}_{\rm corr}$	*n*	[Ca I/H]	rms	err	*n*	...
...	...	...	...	...	...	...	...	...	...	...	...
HD47001	...	−0.20	0.09	0.09	−0.26	14	−0.25	0.05	0.06	11	...
HD73898	...	−0.30	0.03	0.03	−0.28	14	−0.32	0.04	0.05	11	...
HD16815	...	−0.16	0.07	0.07	−0.20	15	−0.25	0.04	0.06	12	...
...	...	...	...	...	...	...	...	...	...	...	...

Notes. *The [*X*/H] abundances after correction for the $T_{\rm eff}$ trends.

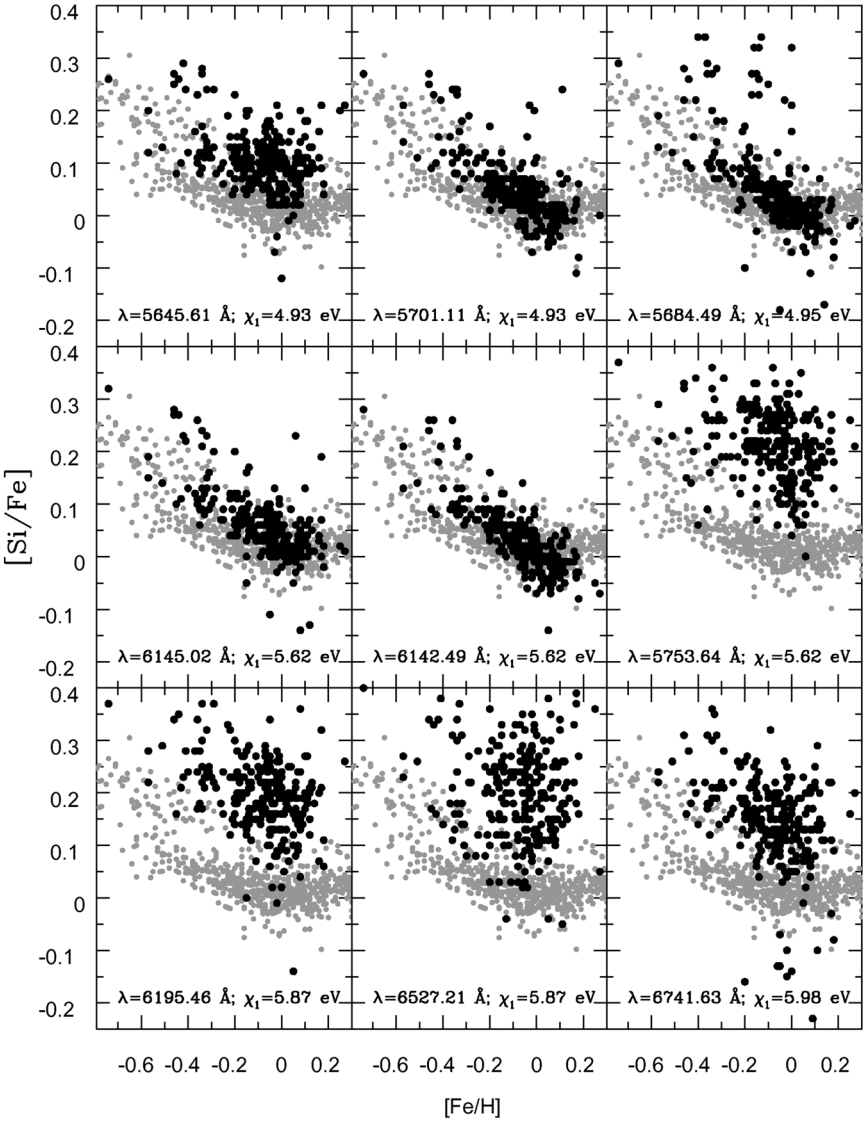

Figure 4. [Si/Fe] versus [Fe/H] plots for Si lines of different EP. The black dots represent the stars of the sample and the grey small dots represent stars from Adibekyan et al. (2012a) with $T_{\rm eff} = T_{\odot} \pm 500$ K. The wavelength of each line and excitation energy of the lower energy level (χ_1) is identified in the lower-left corner of the respective plot.

at solar metallicities, does not depend strongly on the surface gravity and only significant at temperatures above 6500 K (Menzhevitski et al. 2012).

The next element for which we obtained small, but systematic difference between giants and dwarfs is Si. The abundance of Si is not expected to be affected by extra mixing processes in the stars. The few studies of the Si abundances taking into account the non-LTE deviations showed that the effect is significant only at very low metallicities (e.g. Bergemann et al. 2013) and the non-LTE correction for Si of the Sun is about −0.05 dex (Sukhorukov & Shchukina 2012). Since in this study for the Al abundance derivation, we used several lines with different excitation potentials (EP), which means different atmospheric layers of formation and hence different sensitivities to non-LTE deviations, we decided to analyse [Si/Fe] against [Fe/H] for each individual line. In Fig. 4, we plot [Si/Fe] against [Fe/H] for nine Si lines with the lowest, intermediate and highest excitation energy of the lower energy level (χ_1). At the first glance, it looks like the lines with the highest χ_1 show the highest deviations from the abundances derived for the FGK dwarfs. However, as can be seen in the middle panel of the plot the three lines with exactly the same χ_1 show different behaviour, for λ 5753.64 Å showing the largest difference.

Fig. 4 shows that the picture is complex and probably several process (non-LTE, unresolved blends) are acting and affecting the abundances at the same time. To select the 'best' lines i.e. lines which give similar average abundances to that obtained for the dwarfs, for all the lines we calculated the average [Si/Fe] abundance ratio obtained for all the giants with solar metallicity ± 0.1 dex and compared that with the average [Si/Fe] obtained for dwarfs (Adibekyan et al. 2012a) with metallicities in the range of 0.0 ± 0.1 dex. Then we used the rms (scatter) of the [Si/Fe] calculated for the dwarfs[10] to quantify the observed differences (in n× σ). We found 5 (out of 15) Si lines which give [Si/Fe] abundance similar to

[10] The scatter obtained for the dwarfs by averaging the abundance of many lines is more realistic than the scatter obtained from one spectral line for giant stars.

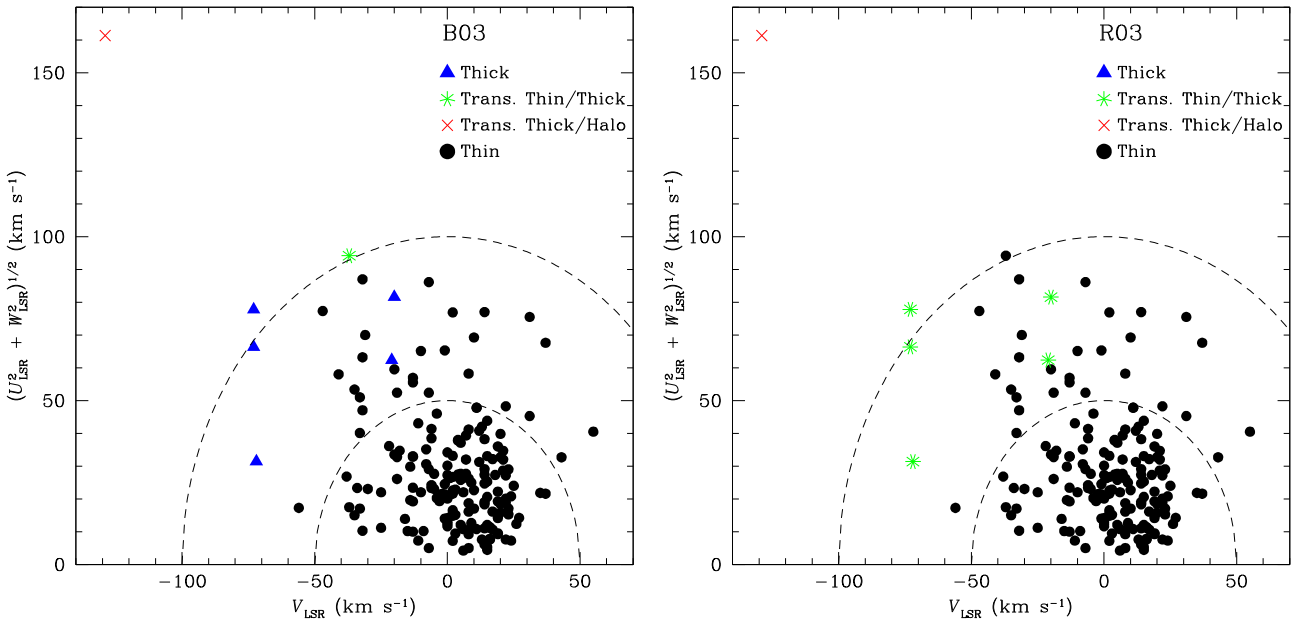

Figure 5. Toomre diagram for the entire sample. The left- and right-hand panels show the separation of the stellar groups according to the Bensby, Feltzing & Lundström (2003, B03) and Robin et al. (2003, R03) prescription, respectively. The symbols are explained in the figure.

that obtained for the dwarfs (less than 2σ difference). The [Si/Fe] abundance obtained by averaging the abundances of the mentioned five lines against [Fe/H] is presented in the Fig. B3. We note that we do not claim that these selected lines are not affected by non-LTE effects of unresolved blends, but they provide abundances similar to that obtained for dwarfs, which probably means that they are more realistic.

We repeated the aforementioned procedure for all the lines for each element and calculated the difference in [$X_{\rm line}$/Fe] between giants and dwarfs for each line. This differences, in n$\times\,\sigma$, is presented in the last column of the line-list table (available at CDS). The [*X*/Fe] versus [Fe/H] relation obtained by using only the 'best' lines (less than 2σ difference) is shown in Fig. B3. The corresponding [*X*/H] abundances are available at CDS.

4 KINEMATICS AND STELLAR POPULATIONS

It is becoming increasingly clear that a separation of the Galactic stellar components based only on stellar abundances is superior to kinematic separation (e.g. Adibekyan et al. 2011; Lee et al. 2011; Navarro et al. 2011; Liu & van de Ven 2012; Recio-Blanco et al. 2014), because chemistry is a relatively more stable property of a star than its spatial positions and kinematics. However, as mentioned above, some changes in abundances of some elements are expected when the stars are evolving and leaving the main sequence. In this analysis, to separate the thin- and thick-disc stellar components, we used the position of the stars in the [α/Fe]–[Fe/H] plane (here α refers to the average abundance of Mg, Si, and Ti), but separately also a kinematics approach is applied.

The space velocity components for 183 stars out of 257 were derived with respect to the local standard of rest, adopting the standard solar motion ($U_\odot$, $V_\odot$, $W_\odot$) = (11.1, 12.24, 7.25) km s^{-1} of Schönrich, Binney & Dehnen (2010). For the remaining 73 stars, we did not calculate the velocities because of the deficit of astrometric literature data. The radial velocities, parallaxes and proper motions were taken from the SIMBAD Astronomical Database.[11] Combining the measurement errors in the parallaxes, proper motions, and radial velocities, the resulting average errors in the U, V, and W velocities are of about 2–3 km s^{-1}.

To assess the likelihood of the stars being a member of different Galactic populations, we followed Reddy, Lambert & Allende Prieto (2006). The probabilities that the stars belong to different stellar populations were calculated, having adopted both the Bensby et al. (2003) and Robin et al. (2003) population fractions. We refer the reader to Adibekyan et al. (2012a) for the details of the computation. The Galactic space velocity components and the probabilities to assign the stellar population to which the stars belong are available at the CDS.

According to the Bensby et al. (2003) criteria, among the 183 stars, we have 176 (96 per cent) stars from the thin disc, 5 from the thick disc, and 2 stars are considered to be transition stars that do not belong to any group. Adopting the criteria from Robin et al. (2003) gives 177 (97 per cent) thin-disc stars, 5 star with kinematics suggesting a thick/thin-disc transition, and one star with a classification of thick-disc/halo transition object. The distribution of the stars in the Tommre diagram is shown in Fig. 5.

As mentioned above, in addition to the difference in their kinematics, the thin- and thick-disc stars are also different in their α content at a given metallicity (e.g. Fuhrmann 1998, 2008). This dichotomy in the chemical evolution allows one to separate different stellar populations.

The [α/Fe] versus [Fe/H] plot for the sample stars along with the dwarf stars from Adibekyan et al. (2012a) with $T_{\rm eff}$ = $T_\odot$ $\pm$ 500 K is depicted in Fig. 6.[12] As one can see from the figure the two samples show similar trends, with giant stars having on average higher [α/Fe] values at a fixed (low) [Fe/H]. This observed difference might arise from our assumption of LTE line formation. The non-LTE effects are stronger for metal-poor stars, but these effects depends also on other stellar parameters (e.g. gravity and

[11] http://simbad.u-strasbg.fr/simbad/

[12] The chemical dissection of the discs is presented in the appendix.

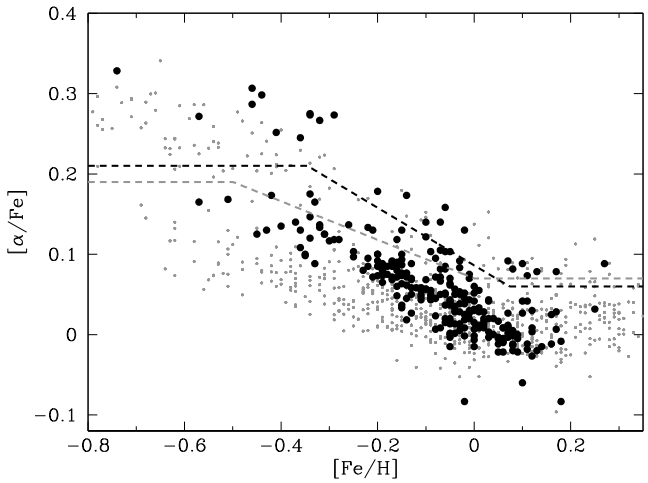

Figure 6. [α/Fe] versus [Fe/H] for the current sample (black dots) and for the stars from Adibekyan et al. (2012a) with $T_{\rm eff} = T_{\odot} \pm 500$ K (grey small dots). The separation between the thick- and thin-disc stars for the two samples are presented in black and grey dashed lines.

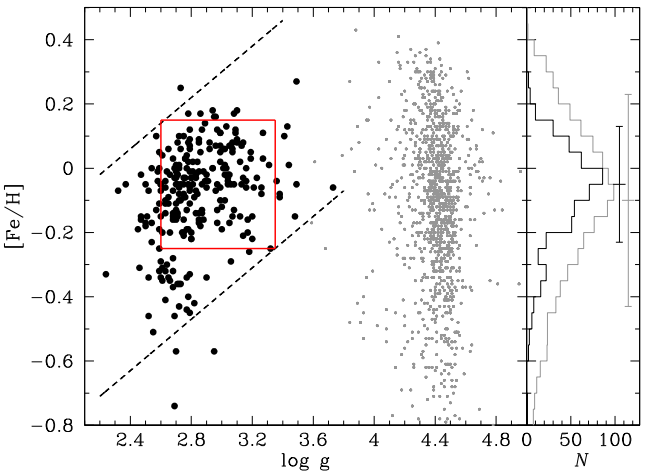

Figure 7. Left-hand panel: [Fe/H] versus log g for the current sample (black dots) and for the stars from Adibekyan et al. (2012a, grey dots). The two black dashed lines were drawn by eye and show the biases in the samples due to the $B - V$ cut-off. Right-hand panel: the metallicity distribution of the two aforementioned samples. The distribution of the giants stars (grey line) was multiplied by 2 for the better visual comparison. The median and its standard deviation are also presented for metallicity distributions of both giants and dwarfs.

temperature) and also they are different for different elements and they differ from line to line. Thus, for fully understanding of the main reason of the observed abundance difference between giants and dwarfs, a complete non-LTE analysis is needed.

Our chemical separation of the Galactic discs suggests that 23 stars (9 per cent) in the sample show enhanced α-abundances. In Adibekyan et al. (2011, 2013), the high-α stars were separated into two groups with a gap in both [α/Fe] and metallicity. It is interesting to see that the gap in [Fe/H] for high-α stars can be also seen in our sample at the same metallicity ($\approx -0.2/-0.3$ dex). Following the same logic and definitions as in Adibekyan et al. (2013), the 10 stars with enhanced [α/Fe] and [Fe/H] below -0.3 dex can be classified as thick-disc stars, and the remaining 13 stars as high-α metal-rich stars (hαmr). With this definition, we see that 4 per cent of the stars belong to the Galactic thick disc, as the kinematic separation was suggesting.

We note that the current sample is small and we will avoid of a definite conclusion about the existence of the mentioned 'gap' at [Fe/H] ≈ -0.3 dex and the distinction of the two α-enhanced metal-poor and metal-rich populations. However, the fact that the two different homogeneously analysed samples (the current one and the one from Adibekyan et al. 2011) show quite similar features probably is more than just a hint about the existence of the hαmr stars as a distinct stellar family. Moreover, recent study of an inner disc metal-rich open cluster, Berkeley 81, shows that the stars are enhanced in α-element Magrini et al. (2015), thus confirming that the hαmr stars have inner disc origin as suggested by Adibekyan et al. (2013). However, we want to note that no similar 'gap' was found in Bensby, Feltzing & Oey (2014) where the authors suggested that the hαmr stars present the metal-rich tail of the thick disc. As mentioned in Bensby et al. (2014), a large sample with well-controlled selection function (e.g. *Gaia*-ESO survey – Gilmore et al. 2012) would help us to understand the real nature of the hαmr stars.

5 METALLICITY DISTRIBUTION

As mentioned above, several authors tried to understand the reason why the apparent giant-planet–metallicity correlation does not exist for evolved stars. As recently suggested by Mortier et al. (2013c), a possible reason might be a selection bias due to $B - V$ colour cut-off.

In Fig. 7, we plotted the relation between stellar metallicity and surface gravity. For the comparison, the dwarf stars sample from Adibekyan et al. (2012a) is also presented. From the figure, one can easily see that the giant stars sample lacks high-metallicity and low-gravity stars, and also low-metallicity and high-gravity stars. This is again probably because of the selection criteria used to define the sample.

To avoid the issues related to the selection effects, an unbiased giant sample with no colour cut-off and homogeneously derived parameters is needed that is systematically searched for planetary companions. However, it is still possible to overcome the effect of the $B - V$ colour cut-off if one considers, for example, only stars in the 'cut rectangle' shown in Fig. 7 (red rectangle), where the stars are equally distributed. However, these 'cut rectangles' will consist of stars with narrower ranges of metallicities (from -0.25 to 0.15 dex in the example of Fig. 7), which is also an issue since the giant-planet–metallicity correlation is more pronounced at high metallicities (at least for dwarf stars).

In the right-hand panel of Fig. 7, we show the metallicity distribution of giant and dwarf stars where narrower [Fe/H] distribution of giants is apparent. The figure also shows that the two distributions are peaked at similar metallicities, close to the solar value. The median (and its standard deviation) of the metallicity distributions of giant and dwarf stars are -0.05 (0.18) and -0.10 (0.33) dex, respectively.[13] Several studies have already observed this tendency of evolved stars lacking the metal-rich and very metal-poor tails (e.g. Taylor & Croxall 2005; Luck & Heiter 2007; Takeda et al. 2008; Ghezzi et al. 2010).

The stars in this sample have stellar masses between 1.5 and 4.0 $M_{\odot}$ (Alves et al. 2015), and hence should be on average younger

[13] We note that the standard deviation of the median is calculated as $1.25*\sigma$, where σ is the standard deviation of the distribution.

than the dwarfs from Adibekyan et al. (2012a). The younger age together with the age–metallicity dispersion relation (e.g. da Silva et al. 2006; Haywood 2008; Casagrande et al. 2011; Maldonado et al. 2013) might explain the narrower [Fe/H] distribution of the giants. Young stars are mostly local since they do not have time to migrate within the Galaxy (Wang & Zhao 2013; Minchev, Chiappini & Martig 2013). Radial migration in the disc is expected to make the metallicity distribution wider, but does not change the mean abundance (Wang & Zhao 2013), as we see in Fig. 7. This is because mostly massive stars contribute to the chemical enrichment of the interstellar medium and they contribute mainly around their birth places because of their very short lifetime. The lack of very metal-rich giants can be understood along the same migration process, most of the old stars which migrate would come from the inner, metal-rich disc (Minchev et al. 2013; Wang & Zhao 2013).

In addition to the aforementioned astrophysical explanation, we would like to note again the selection effects which may arise in evolved star samples due to $B - V$ colour cut-off. This selection bias may also make the metallicity distribution narrower.

6 SUMMARY OF THE RESULTS

We have carried out a uniform abundance analysis for 12 refractory elements for a sample of 257 field G-, K-type evolved stars that are being surveyed for planets using precise radial–velocity measurements with the CORALIE spectrograph. The abundances were derived using a carefully selected line-list and are based on the precise spectroscopic parameters derived by Alves et al. (2015) using the same spectra as were used in the present study.

We found that for all the elements Galactic chemical evolution trends are similar for giant and dwarf stars, while for some species [*X*/Fe] values are shifted towards higher values at a fixed metallicity. Our LTE analysis confirms the overabundance of Na in giant stars compared to the field FGK dwarf stars from Adibekyan et al. (2012a). This overabundance may have a stellar evolutionary character, even though the possible departures from non-LTE may produce an enhancement of a similar degree (Alexeeva et al. 2014). We showed that an observed small overabundance of Si compared to the field FGK dwarf vanishes when a shorter, carefully select line-list is used.

To separate Galactic stellar populations, we applied both a purely kinematical approach and chemical method. Our chemical separation suggests that 91 per cent of the stars, being α-poor, belong to the thin disc and the remaining 9 per cent of the stars show enhanced α-element abundances at a fixed [Fe/H]. This sample (while being not very large) also suggests a 'gap' in [Fe/H] for high-α stars as observed in Adibekyan et al. (2011). Following the definition of the last authors, 4 per cent of the stars were classified as thick-disc members (being metal-poor) and 5 per cent as hαmr stars.

The metallicity distribution of the giant stars is shown to be narrower than that of their non-evolved dwarf counterparts (see also Taylor & Croxall 2005; Takeda et al. 2008), but peaked at almost solar metallicity as in case of the dwarfs. The lack of very metal-rich and metal-poor stars can be explained by the fact that most of the stars are originated in the solar vicinity. Evolved stellar samples mostly consist of massive stars, which have shorter lifetime than the dwarfs, and therefore do not have enough time to migrate from further inner/outer discs (Minchev et al. 2013; Wang & Zhao 2013).

Our present sample, as most of the giant star samples searched for planets, is affected by $B - V$ colour cut-off which excludes low-log g stars with high [Fe/H] and high-log g stars with low metallicity. As discussed in Mortier et al. (2013c), this selection bias might be the reason of the absence of the correlation between occurrence of giant-planet planets and stellar metallicity. We suggest to use stars in a 'cut-rectangle' in the log g–[Fe/H] diagram to overcome the aforementioned issue, if an unbiased sample is not available on hand.

Although the current sample still contains only one star known to orbit a planetary companion (HD 11977 – Setiawan et al. 2005), most of the stars have already been periodically observed over the last years. Before a significant number of planets are detected, this sample can be used as a homogeneous comparison sample to study planet occurrence around giant stars. However, when exploring chemical peculiarities of planet-hosting giant stars, one should bear in mind the chemical properties of these evolved stars discussed in this paper (e.g. enhancement in Na, Al, etc.).

ACKNOWLEDGEMENTS

This work was supported by the European Research Council/European Community under the FP7 through Starting Grant agreement number 239953. This work was also supported by the Gaia Research for European Astronomy Training (GREATITN) Marie Curie network, funded through the European Union Seventh Framework Programme ([FP7/2007-2013]) under grant agreement number 264895. V.Zh.A. and S.G.S acknowledge the support from the Fundação para a Ciência e a Tecnologia, FCT (Portugal) in the form of the fellowships SFRH/BPD/70574/2010 and SFRH/BPD/47611/2008, respectively. NCS was supported by FCT through the Investigator FCT contract reference IF/00169/2012 and POPH/FSE (EC) by FEDER funding through the programme 'Programa Operacional de Factores de Competitividade' – COMPETE. Research activities of the Observational Stellar Board of the Federal University of Rio Grande do Norte are supported by continuous grants of CNPq and FAPERN Brazilian agencies and by the INCT-INEspao. SA acknowledges Post-Doctoral Fellowship from the CAPES brazilian agency (BEX-2077140), and also support by Iniciativa Científica Milenio through grant IC120009, awarded to The Millennium Institute of Astrophysics. GI acknowledges financial support from the Spanish Ministry project MINECO AYA2011-29060. AM received funding from the European Union Seventh Framework Programme (FP7/2007-2013) under grant agreement number 313014 (ETAEARTH). This research has made use of the SIMBAD database operated at CDS, Strasbourg, France. We thank Mahmoudreza Oshagh for his interesting comments related to Fig. 6, and Elisa Delgado Mena for a very constructive discussion. We would also like to thank the anonymous referee for useful comments that helped to improve the paper.

REFERENCES

Adibekyan V. Zh., Santos N. C., Sousa S. G., Israelian G., 2011, A&A, 535, L11

Adibekyan V. Zh., Sousa S. G., Santos N. C., Delgado Mena E., González Hernández J. I., Israelian G., Mayor M., Khachatryan G., 2012a, A&A, 545, A32

Adibekyan V. Zh., Delgado Mena E., Sousa S. G., Santos N. C., Israelian G., Gonzlez Hernndez J. I., Mayor M., Hakobyan A. A., 2012b, A&A, 547, A36

Adibekyan V. Zh. et al., 2013, A&A, 554, A44

Alexeeva S. A., Pakhomov Y. V., Mashonkina L. I., 2014, Astron. Lett., 40, 406

Allende Prieto C., Barklem P. S., Lambert D. L., Cunha K., 2004, A&A, 420, 183
Alves S. et al., 2015, MNRAS, 448, 2749
Anders E., Grevesse N., 1989, Geochim. Cosmochim. Acta, 53, 197
Baumueller D., Gehren T., 1996, A&A, 307, 961
Baumueller D., Gehren T., 1997, A&A, 325, 1088
Bensby T., Feltzing S., Lundström I., 2003, A&A, 410, 527
Bensby T., Feltzing S., Oey M. S., 2014, A&A, 562, A71
Bergemann M., 2011, MNRAS, 413, 2184
Bergemann M., Kudritzki R.-P., Würl M., Plez B., Davies B., Gazak Z., 2013, ApJ, 764, 115
Bergemann M., Kudritzki R.-P., Davies B., 2014, preprint (arXiv:1403.3087)
Casagrande L., Schönrich R., Asplund M., Cassisi S., Ramírez I., Meléndez J., Bensby T., Feltzing S., 2011, A&A, 530, A138
da Silva L. et al., 2006, A&A, 458, 609
Figueira P., Santos N. C., Pepe F., Lovis C., Nardetto N., 2013, A&A, 557, A93
Fischer D. A., Valenti J., 2005, ApJ, 622, 1102
Friel E. D., Jacobson H. R., Barrett E., Fullton L., Balachandran S. C., Pilachowski C. A., 2003, AJ, 126, 2372
Friel E. D., Jacobson H. R., Pilachowski C. A., 2005, AJ, 129, 2725
Fuhrmann K., 1998, A&A, 338, 161
Fuhrmann K., 2008, MNRAS, 384, 173
Ghezzi L., Cunha K., Schuler S. C., Smith V. V., 2010, ApJ, 725, 721
Gilmore G. et al., 2012, The Messenger, 147, 25
Gonzalez G., 1997, MNRAS, 285, 403
Haywood M., 2008, MNRAS, 388, 1175
Hekker S., Meléndez J., 2007, A&A, 475, 1003
Jacobson H. R., Friel E. D., Pilachowski C. A., 2007, AJ, 134, 1216
Jofré E., Petrucci R., Saffe C., Saker L., de la Villarmois E. A., Chavero C., Gómez M., Mauas P. J. D., 2015, A&A, 574, A50
Johnson J. A., Aller K. M., Howard A. W., Crepp J. R., 2010, PASP, 122, 905
Kurucz R., 1993, Kurucz CD-ROM No. 13. Smithsonian Astrophysical Observatory, Cambridge, MA
Lee Y. S. et al., 2011, ApJ, 738, 187
Liu C., van de Ven G., 2012, MNRAS, 425, 2144
Liu Y. J., Zhao G., Shi J. R., Pietrzyński G., Gieren W., 2007, MNRAS, 382, 553
Luck R. E., Heiter U., 2007, AJ, 133, 2464
Maldonado J., Villaver E., Eiroa C., 2013, A&A, 554, A84
Menzhevitski V. S., Shimansky V. V., Shimanskaya N. N., 2012, Astrophys. Bull., 67, 294
Minchev I., Chiappini C., Martig M., 2013, A&A, 558, A9
Magrini L. et al., 2015, A&A, submitted
Mortier A., Santos N. C., Sousa S. G., Fernandes J. M., Adibekyan V. Z., Delgado Mena E., Montalto M., Israelian G., 2013a, A&A, 558, 106A
Mortier A., Santos N. C., Sousa S., Israelian G., Mayor M., Udry S., 2013b, A&A, 551, 112A
Mortier A., Santos N. C., Sousa S. G., Adibekyan V. Z., Delgado Mena E., Tsantaki M., Israelian G., Mayor M., 2013c, A&A, 557, A70
Navarro J. F., Abadi M. G., Venn K. A., Freeman K. C., Anguiano B., 2011, MNRAS, 412, 1203
Neves V., Santos N. C., Sousa S. G., Correia A. C. M., Israelian G., 2009, A&A, 497, 563
Nissen P. E., 1981, A&A, 97, 145
Pasquini L., Döllinger M. P., Weiss A., Girardi L., Chavero C., Hatzes A. P., da Silva L., Setiawan J., 2007, A&A, 473, 979
Petigura E. A., Marcy G. W., 2011, ApJ, 735, 41
Quirrenbach A., Reffert S., Bergmann C., 2011, in Schuh S., Drechsel H., Heber U., eds, AIP Conf. Proc. Vol. 1331, Planets around Giant Stars. Am. Inst. Phys., New York, p. 102
Ramírez I., Allende Prieto C., Lambert D. L., 2013, ApJ, 764, 78
Recio-Blanco A. et al., 2014, A&A, 567, A5
Reddy B. E., Lambert D. L., Allende Prieto C., 2006, MNRAS, 367, 1329
Reffert S., Bergmann C., Quirrenbach A., Trifonov T., Künstler A., 2015, A&A, 574, 116A
Robin A. C., Reylé C., Derrière S., Picaud S., 2003, A&A, 409, 523
Santos N. C., Israelian G., Mayor M., 2001, A&A, 373, 1019
Santos N. C., Israelian G., Mayor M., 2004, A&A, 415, 1153
Santos N. C., Lovis C., Pace G., Melendez J., Naef D., 2009, A&A, 493, 309
Santrich O. J. K., Pereira C. B., Drake N. A., 2013, A&A, 554, A2
Schönrich R., Binney J., Dehnen W., 2010, MNRAS, 403, 1829
Setiawan J. et al., 2005, A&A, 437, L31
Sneden C. A., 1973, PhD thesis, Univ. Texas, Austin
Sousa S. G., 2014, preprint (arXiv:1407.5817)
Sousa S. G., Santos N. C., Israelian G., Mayor M., Monteiro M. J. P. F. G., 2007, A&A, 469, 783
Sousa S. G. et al., 2008, A&A, 487, 373
Sousa S. G., Santos N. C., Israelian G., Mayor M., Udry S., 2011, A&A, 533, A141
Sukhorukov A. V., Shchukina N. G., 2012, Kinematics Phys. Celest. Bodies, 28, 169
Takeda Y., Sato B., Murata D., 2008, PASJ, 60, 781
Tautvaišienė G., Edvardsson B., Puzeras E., Ilyin I., 2005, A&A, 431, 933
Taylor B. J., Croxall K., 2005, MNRAS, 357, 967
Tsantaki M., Sousa S. G., Adibekyan V. Z., Santos N. C., Mortier A., Israelian G., 2013, A&A, 555, A150
Udry S. et al., 2000, A&A, 356, 590
Valenti J. A., Fischer D. A., 2005, ApJS, 159, 141
Villanova S., Carraro G., Saviane I., 2009, A&A, 504, 845
Wang Y., Zhao G., 2013, ApJ, 769, 4

APPENDIX A: INTERDEPENDENCE OF STELLAR PARAMETERS AND THE MICROTURBULENCE

The interdependence of the fundamental parameters is presented in Fig. A1. The figure reveals several interesting correlations between the parameters, for instance one can see that the metallicity correlates with surface gravity (see also Section 5) and also stars with higher $T_{\rm eff}$ (above 5100 K) show higher metallicity. Microturbulent velocity correlates with the $\log g$. The significance of the observed correlations is estimated following the method described in Figueira et al. (2013) and Adibekyan et al. (2013), and the parameters of the linear relations are presented in Table A1. We note that five stars classified as 'outliers' in the $\xi_{\rm t}$–$\log g$, were excluded from the estimation of the significance of the correlations (see the next section for details).

A1 The microturbulence relationship

Sometimes, when the number of iron lines is not large enough, a correct determination of microturbulence becomes very difficult because of small EW interval of the Fe I lines (e.g. Mortier et al. 2013b). In these cases, one uses empirically obtained relations between microturbulence and other stellar parameters. Several studies have shown that for FGK dwarf stars, microturbulent velocity depends on $\log g$ and $T_{\rm eff}$ (e.g. Nissen 1981; Allende Prieto et al. 2004; Adibekyan et al. 2012b; Ramírez, Allende Prieto & Lambert 2013; Tsantaki et al. 2013). Takeda et al. (2008) has already suggested that the microturbulence correlates with the surface gravity; however, the authors did not provide the analytic form of the relation.

To find out the parameters the $\xi_{\rm t}$ correlates with, we first applied a linear fit for three pairs of data sets: $\xi_{\rm t}$–[Fe/H], $\xi_{\rm t}$–$\log g$, $\xi_{\rm t}$–$T_{\rm eff}$. Then we evaluated the significance of the correlation, by using a bootstrap procedure as it was done in Figueira et al. (2013). As expected the strongest correlation is observed with $\log g$ (5.7σ), $\approx 4\sigma$ in case of $T_{\rm eff}$, and $\approx 1.8\sigma$ for [Fe/H]. However, the fits can be affected by the presence of several outliers as can be seen in Fig. A1. To remove the outliers, we used the $\xi_{\rm t}$–$\log g$ relation (since

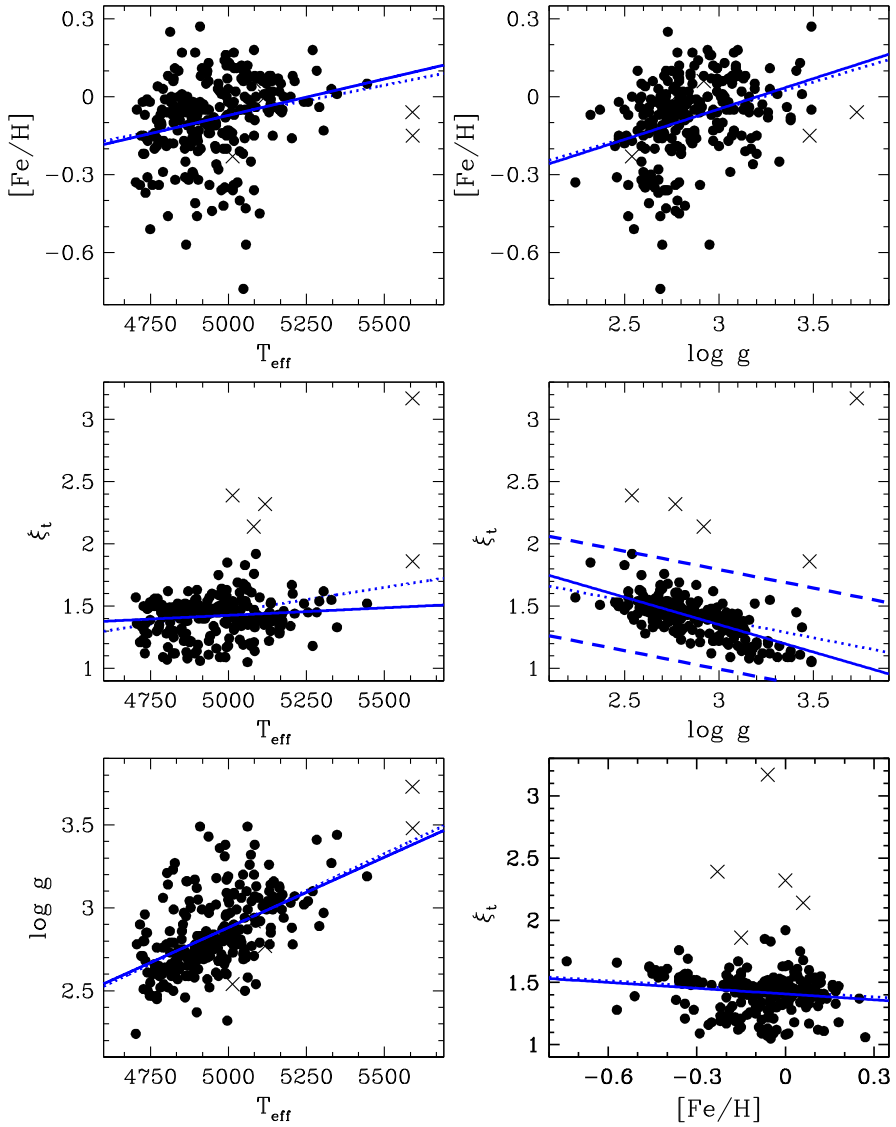

Figure A1. Interdependence of the stellar atmospheric parameters of the sample stars. The blue dotted lines depict the linear fits of the full data, and the sold lines are the fits after removing five 'outliers'. The 2σ intervals of the linear fit of the ξ_t–log g relation are shown in blue dashed lines. The black crosses indicate the five outliers.

Table A1. The coefficients of the linear fits ($y = a \times X + b$) of the relations between the stellar parameters, along with the correlation coefficient and the significance. The number of stars is 251.

Elem	a	b	R^2	z-score
ξ_t–$T_{\rm eff}$	0.120 ± 0.065	0.825 ± 0.326	0.013	1.7
log g–$T_{\rm eff}$	0.847 ± 0.089	− 1.356 ± 0.441	0.266	7.9
[Fe/H]–$T_{\rm eff}$	0.280 ± 0.069	− 1.472 ± 0.343	0.061	3.9
[Fe/H]–log g	0.234 ± 0.041	− 0.751 ± 0.116	0.116	5.4
ξ_t–log g	− 0.440 ± 0.029	2.673 ± 0.083	0.476	10.8
ξ_t–[Fe/H]	− 0.154 ± 0.057	1.407 ± 0.010	0.027	2.6

it shows the strongest correlation), by applying 2σ-clipping (two times of residual standard deviation). Then, after cleaning the data from outliers we again fitted the data and again evaluated the significance of the relations. We found that microturbulence significantly correlated with the surface gravity (at about 11σ level), and with the metallicity but with less degree of significance. The five outliers were responsible for the 'strong' relation observed between ξ_t and $T_{\rm eff}$.

After this test, we decided to present the relation of microturbulence only with log g and [Fe/H], which has the following functional form:

$$\xi_t = 2.72(\pm0.08) - 0.457(\pm0.031) \times \log g + 0.072(\pm0.044) \times [\mathrm{Fe/H}] \quad \text{(A1)}$$

We note that this empirical relation is valid only for the range of stellar parameters that the stars in our sample cover.

APPENDIX B: [*X*/FE] DEPENDENCE ON STELLAR PARAMETERS

In this section, we present [*X*/Fe] versus log g (Fig. B1), [*X*/Fe] versus microturbulence (Fig. B2), and [*X*/Fe] versus [Fe/H] (Fig. B3) plots derived from the 'best' lines as discussed in the main text.

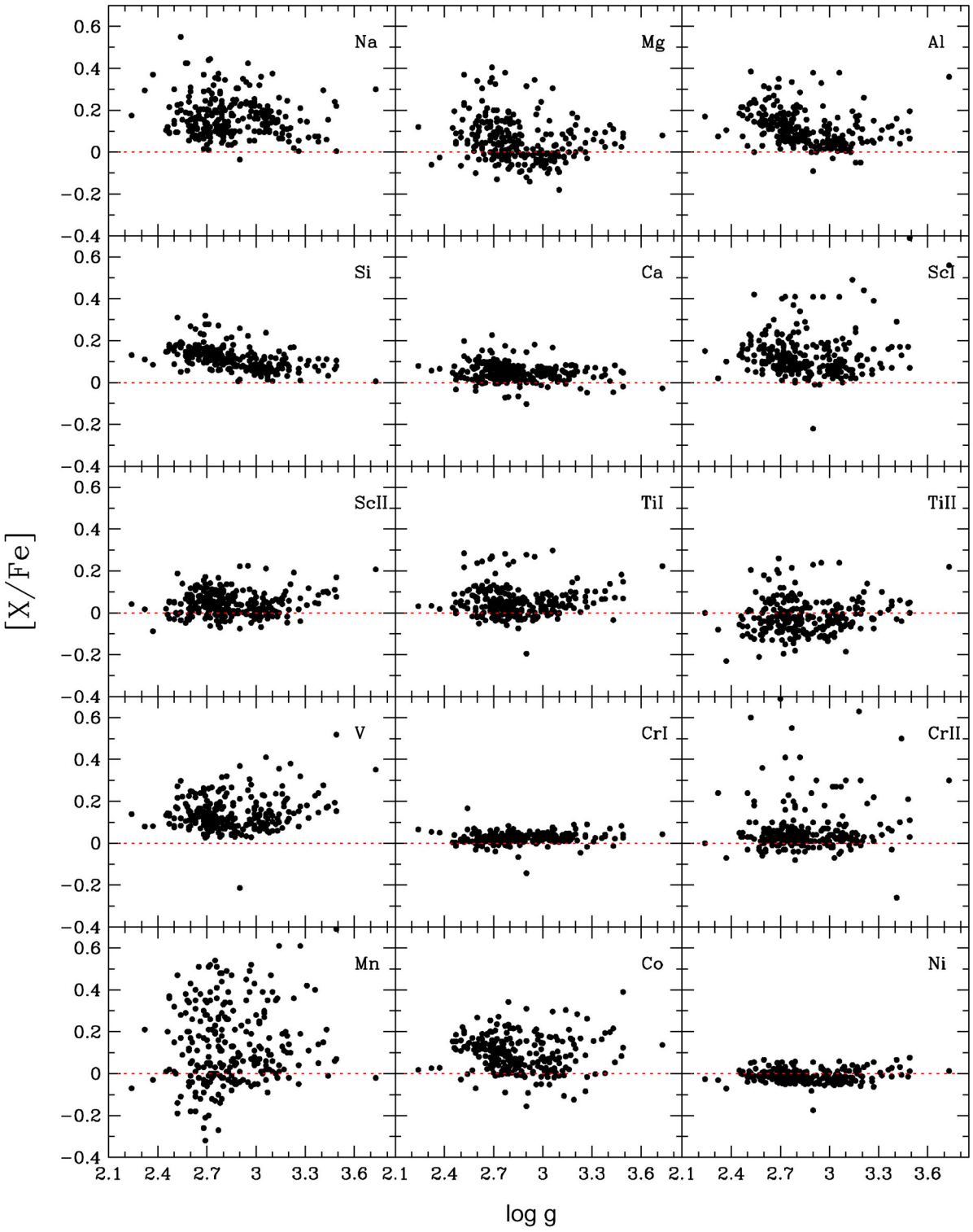

Figure B1. [*X*/Fe] versus log *g* plots. Each element is identified in the upper-right corner of the respective plot. The black dots represent the stars of the current sample.

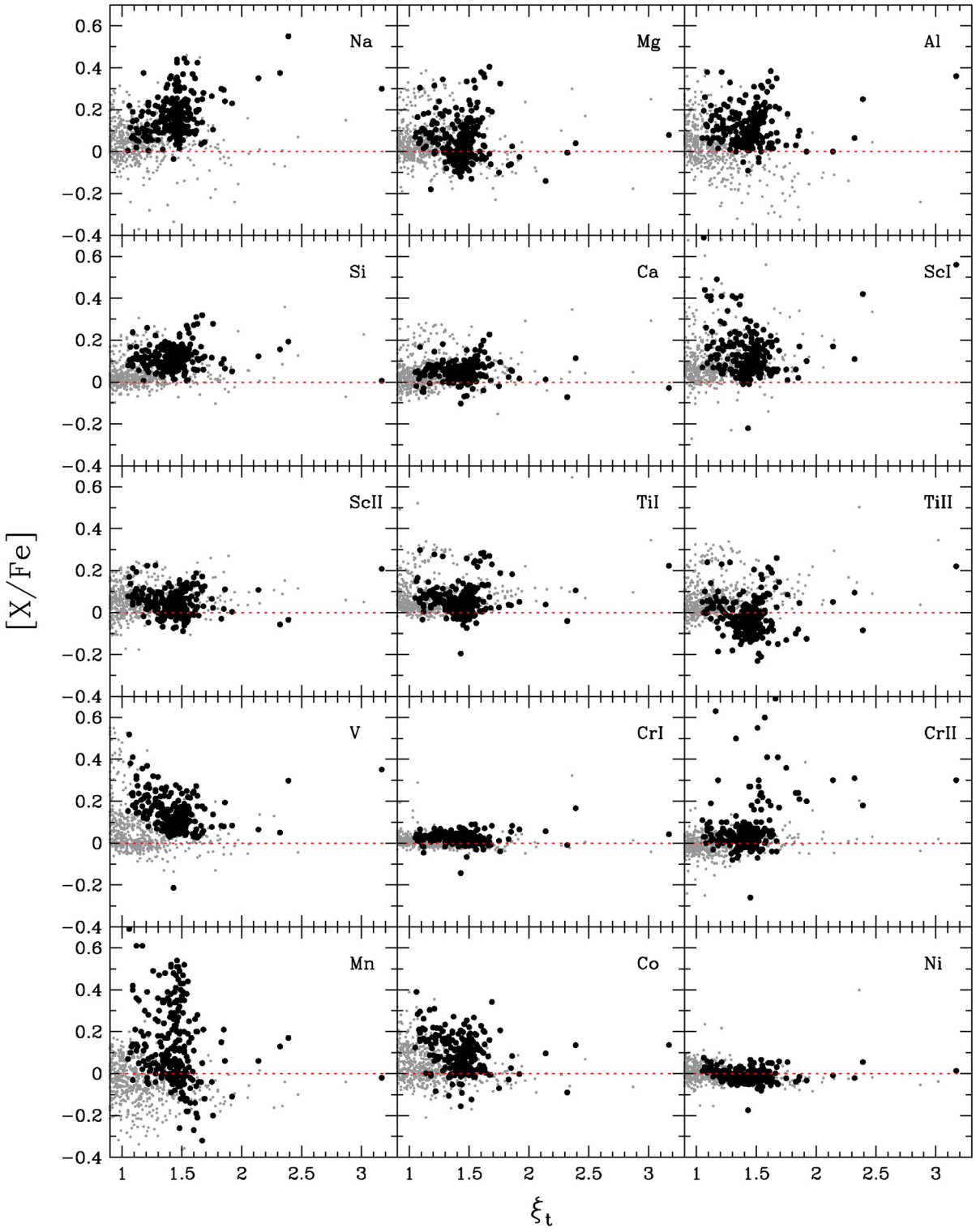

Figure B2. [*X*/Fe] versus microturbulence plots. Each element is identified in the upper-right corner of the respective plot. The black dots represent the stars of the sample and the grey small dots represent stars from Adibekyan et al. (2012a).

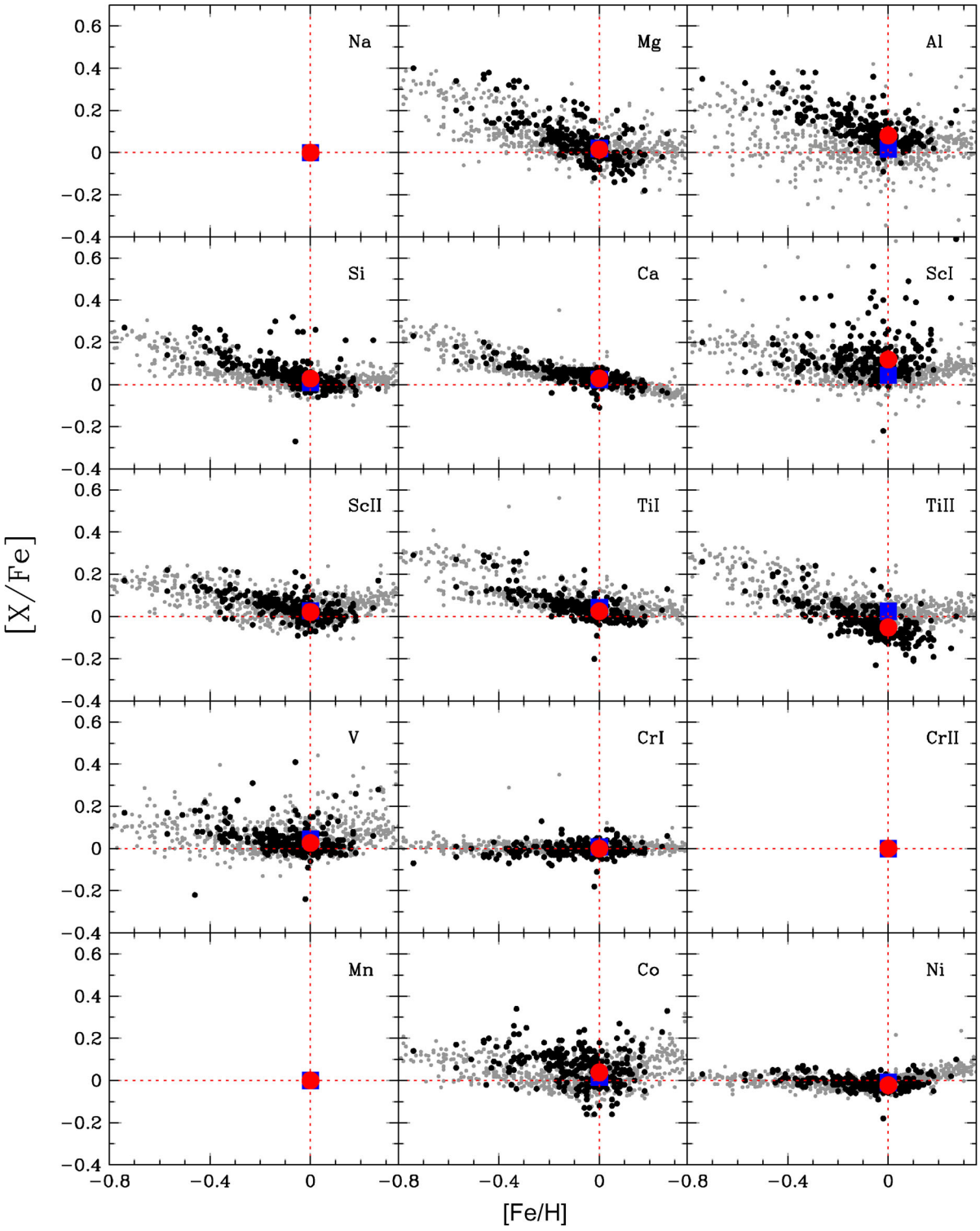

Figure B3. [*X*/Fe] versus [Fe/H] plots derived from the 'best' lines. For Na I, Cr II, and Mn I there was no 'best' line(s) found. The black dots represent the stars of the sample and the grey small dots represent stars from Adibekyan et al. (2012a) with $T_{\rm eff} = T_{\odot} \pm 500$ K. The red circle and blue square show the average [*X*/Fe] value of stars with [Fe/H] $= 0.0 \pm 0.1$ dex. Each element is identified in the upper-right corner of the respective plot.

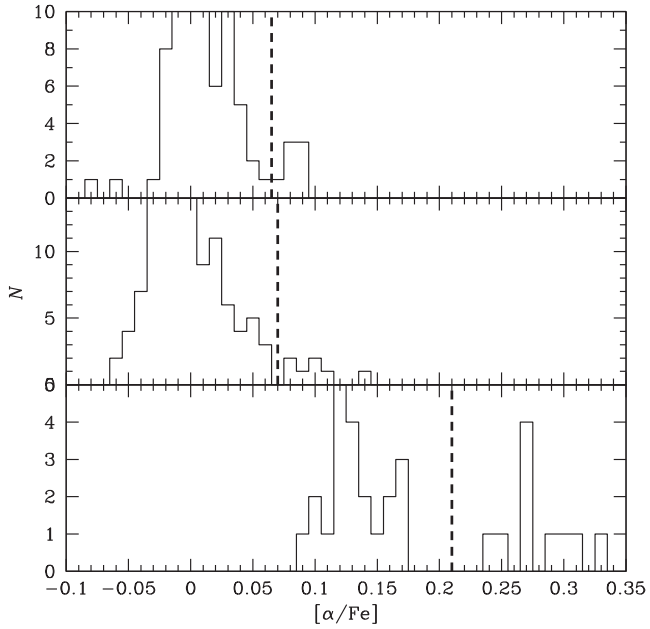

Figure C1. High-α and low-α separation histograms for the stars with metallicities < -0.3 dex (bottom), $-0.3 \leq$ [Fe/H] ≤ 0.0 dex (middle), and [Fe/H] > 0.0 dex (top). The dotted lines are the separation curves between the thin and thick discs.

APPENDIX C: SEPARATION OF THE GALACTIC DISCS BY α-ENHANCEMENT

For the separation of Galactic stellar population by the chemical properties of the stars was done following the method presented in Adibekyan et al. (2011). We first divided the sample into three metallicity bins: [Fe/H] < -0.3 dex, [Fe/H] > 0.0 dex, and stars in between. For the lowest and highest metallicity bins, we easily identified the minima in the [α/Fe] histograms. For the intermediate metallicity, stars just plotting the [α/Fe] histogram will not reveal the minima, because the stars at these metallicities show a decrease of [α/Fe] with [Fe/H] (see Fig. C1). Thus, we first detrended the [α/Fe] by applying a liner fit and subtracting it. Then in the [α/Fe] histogram we identified the minima and by adding it to the previously applied liner fit we obtained the line which separates the high- and low-α stars at $-0.3 \leq$ [Fe/H] $\leq$ 0.0 dex. The separation lines for each metallicity bin presented in Fig. C1.

This paper has been typeset from a TEX/LATEX file prepared by the author.